Molecular Determinants of Tissue Specificity of Flavivirus Nonstructural Protein 1 Interaction with Endothelial Cells

Nicholas T.N. Lo, Susan Roodsari, Nicole R. Tin, Scott B. Biering*, Eva Harris*

Division of Infectious Disease and Vaccinology, School of Public Health

University of California, Berkeley, Berkeley, CA, USA

*Correspondence:

Eva Harris, PhD (eharris@berkeley.edu); Scott B. Biering, PhD (sbiering@berkeley.edu)

Division of Infectious Disease and Vaccinology

510 Li Ka Shing Biomedical Center

School of Public Health

University of California, Berkeley

Berkeley, CA 94720, USA

Abstract:

Members of the mosquito-borne flavivirus genus such as dengue (DENV), West Nile (WNV), and Zika (ZIKV) viruses cause distinct diseases and affect different tissues. We previously found that the secreted flaviviral nonstructural protein 1 (NS1) interacts with endothelial cells and disrupts endothelial barrier function in a tissue-specific manner consistent with the disease tropism of the respective viruses. However, the underlying molecular mechanism of this tissue-specific NS1-endothelial cell interaction is not well understood. To elucidate the distinct role(s) that the domains of NS1 (β-roll, wing, and β-ladder) play in NS1 interactions with endothelial cells, we constructed flavivirus NS1 chimeras that exchanged the wing and β-ladder domains in a pair-wise manner between DENV, WNV, and ZIKV NS1. We found that both the NS1 wing and β-ladder domains conferred NS1 tissue-specific endothelial dysfunction, with the wing conferring cell binding and the β-ladder involved in inducing endothelial hyperpermeability as measured by trans-endothelial electrical resistance assay. To narrow down the amino acids dictating cell binding specificity, we utilized the DENV-WNV NS1 chimera and identified residues 91 to 93 (GDI) of DENV NS1 as a molecular motif determining binding specificity. Further, using an *in vivo* mouse model of localized leak, we found that the GDI motif of the wing domain was essential for triggering DENV NS1-induced vascular leak in mouse dermis. Taken together, we identify molecular determinants of flavivirus NS1 that confer NS1 binding and vascular leak and highlight the importance of the NS1 wing domain for flavivirus pathogenesis.

Importance:

Flavivirus NS1 is secreted into the bloodstream from infected cells during a viral infection. Dengue virus NS1 contributes to severe dengue pathology such as endothelial dysfunction and vascular leak independently of the virus. We have shown that multiple flavivirus NS1 proteins result in endothelial dysfunction in a tissue-specific manner consistent with their respective viral tropism. Here, we aimed to identify the molecular determinants that make some, but not other, flavivirus NS1 proteins bind to select endothelial cells in vitro and cause vascular leak in a mouse model. We identified the wing domain of NS1 as a primary determinant conferring differential endothelial dysfunction and vascular leak and narrowed the contributing amino acid residues to a three-residue motif within the wing domain. The insights from this study pave the way for future studies on the effects of flavivirus NS1 on viral dissemination and pathogenesis and offer potential new avenues for antiviral therapies.

Keywords:

Flavivirus, NS1, endothelial dysfunction, vascular leak, endothelial cells, tissue specificity

Running Title:

Flavivirus NS1 tissue-specific molecular determinants

Introduction

Dengue virus (DENV) is a mosquito-borne positive-stranded RNA virus of the *Flavivirus* genus, consisting of four serotypes (DENV1-4). DENV causes ~100 million symptomatic infections per year globally, ranging from classic dengue fever to the more severe dengue haemorrhagic fever and dengue shock syndrome (1–3). The severe forms of dengue are characterized by clinical presentation of vascular leak as a result of endothelial dysfunction (4). Traditionally, endothelial dysfunction has been attributed to a hyperactivated immune response as a result of uncontrolled viral infection and immune cell activation (5, 6). Recently, we and others have demonstrated that the secreted nonstructural protein 1 (NS1) directly contributes to endothelial dysfunction and vascular leak through interactions with endothelial and immune cells that result in the breakdown of endothelial barriers such as the endothelial glycocalyx and tight and adherens junctions (7–13). In addition to DENV, West Nile (WNV) and Zika (ZIKV) viruses are also members of the *Flavivirus* genus that cause human diseases of public health significance. Like DENV NS1, the NS1 proteins of WNV and ZIKV have also been shown to modulate endothelial barriers. WNV NS1 also has been shown to contribute to WNV infection in the brain (14), while ZIKV NS1 has been shown to modulate the barrier integrity of placental explants as well as the testis (10), contributing to ZIKV infection of Sertoli cells (9, 15).

NS1 is a ~55-kDa glycoprotein that is highly conserved across the flaviviruses (16). It dimerizes in the endoplasmic reticulum and is found as a component of the viral replication complex. The dimers can also trimerize to form hexamers that are secreted by DENV-infected cells into the bloodstream as a soluble lipoprotein containing lipid cargo (17–19). In severe dengue patients, the levels of detectable NS1 in the blood can be as high as 1-10 µg/mL (20, 21). Secreted NS1 has been shown to associate with components of the innate immune system such as toll-like receptors (13, 22) and complement proteins (23–25), as well as components of the blood-clotting cascade such as platelets (26–28), which results in both host immune evasion and modulation of barrier integrity of endothelial cells. Separately, NS1 can also directly disrupt endothelial cell barrier integrity by promoting the degradation of endothelial glycocalyx components that line the surface of endothelial cells (7, 12, 29, 30) and

disrupting junctional proteins that mediate cell-cell interactions (8, 31, 32). In mouse models, NS1 vaccination has been shown to be protective against lethal DENV challenge. In contrast, addition of NS1 to sub-lethal DENV infection was shown to exacerbate pathology resulting in a lethal infection, suggesting the potential of NS1 as a vaccine component and therapeutic target (12).

NS1 proteins from multiple flaviviruses have been shown to interact with endothelial cells of distinct tissue origin in a manner consistent with the tropism of its respective flavivirus (33). For example, DENV NS1 interacts with multiple cell lines including human pulmonary microvascular endothelial cells (HPMEC), which correlates with the systemic nature of DENV infection that can be observed in the lungs. In contrast, WNV NS1 interacts well with brain endothelial cells but minimally with HPMEC, as WNV causes neurological pathologies, such as meningitis and encephalitis, but not pulmonary pathology. Similarly, ZIKV NS1 interacts well with both brain and umbilical vein endothelial cells but minimally with HPMEC, as ZIKV causes neurological and congenital but not pulmonary pathologies. However, how these tissue-specific NS1 interactions are modulated remains unclear.

Flavivirus NS1 contains three domains that are highly conserved: the β-roll (residues 1–29), wing (residues 30–180), and β-ladder (residues 181–352) (34). The NS1 β-roll and wing domains contain many hydrophobic residues that are predicted to interact with the cell's plasma membrane (35, 36). Interestingly, these surface-exposed residues are conserved among DENV serotypes but divergent across the flavivirus genus (e.g. between DENV and WNV), suggesting their possible roles in mediating NS1 tissue-specific interactions. Additionally, prior studies have suggested that the three domains of NS1 may have distinct functions. DENV NS1 wing domain has been shown to be immunodominant (12, 37, 38), where conserved, hydrophobic residues in the flexible loop (residues 108–129) within the wing domain (Trp-115, Trp-118, Gly-119) have been identified to partially contribute to DENV NS1 binding to HPMEC (35, 39). In contrast, select residues in the β-ladder domain (such as residues N207, A303, E326, and E327) have been implicated as important for NS1-induced endothelial hyperpermeability, while being dispensable for binding endothelial cells (31, 39). While these data offer clues about NS1

103 molecular determinants of tissue-specific interactions with endothelial cells, a systematic investigation
104 of these different domains in distinct flavivirus NS1 proteins has not been undertaken.

105 In this study, we provide new insights on the tissue-specific interactions between flavivirus NS1 and
106 endothelial cells using NS1 chimeras that exchange the wing and β-ladder domains of DENV, WNV,
107 and ZIKV in a pair-wise manner with one another. We found that both the wing and β-ladder domains
108 confer tissue-specific barrier dysfunction, with the wing influencing initial attachment to endothelial cells
109 and the β-ladder involved in inducing endothelial hyperpermeability *in vitro*. We further identified a
110 variable 3-amino acid (aa) motif in the wing domain as a molecular determinant for tissue specificity.
111 Finally, we identify the wing domain and the 3-aa motif as a driver of DENV-triggered vascular leak *in*
112 *vivo*. Taken together, our results provide insights into the tissue-specific interactions of flavivirus NS1.

Results

The wing domain of flavivirus NS1 confers binding to endothelial cells

In previous work, we showed that DENV NS1 binds to human lung endothelial cells (HPMEC) at higher levels than WNV and ZIKV NS1 (33), correlating with the capacity of DENV NS1 but not WNV or ZIKV NS1 to cause endothelial hyperpermeability of HPMEC and pleural effusion in humans. Similarly, DENV and ZIKV NS1 exhibited higher binding than WNV NS1 to human umbilical vein microvascular endothelial cells (HUVEC) and caused endothelial hyperpermeability of HUVEC (33). To uncover the molecular determinants of flavivirus NS1 that dictate this tissue-specific endothelial cell tropism, we generated chimeric NS1 proteins that exchanged either the wing or the β-ladder domains between DENV and WNV, WNV and ZIKV, and DENV and ZIKV NS1, respectively (Fig. 1A, D, G). We cloned and expressed the C-terminally His-tagged NS1 proteins in HEK-293 cells, which were successfully secreted, and then purified NS1 oligomers using cobalt affinity chromatography (Fig. 2). Chimeric proteins are annotated by their 3 domains from the respective flavivirus NS1 proteins in sequence "β-roll–wing–β-ladder" (e.g., D-D-W designating DENV β-roll – DENV wing – WNV β-ladder). We treated HPMEC with either wild-type (WT) or DENV-WNV chimeric NS1 proteins and measured the levels of NS1 binding to HPMEC using an immunofluorescence microscopy assay (IFA). We found that the chimeric NS1 constructs containing DENV NS1 wing domain bound to HPMEC at comparable levels to WT DENV NS1, whereas the constructs containing WNV NS1 wing exhibited significantly lower binding than WT DENV NS1, but at comparable levels to WT WNV NS1 (Fig. 1B, C). A similar pattern was observed when we treated HUVEC with WNV-ZIKV chimeric NS1, where constructs that contained ZIKV NS1 wing bound to HUVEC at comparable levels to WT ZIKV NS1, whereas the constructs containing WNV NS1 wing bound to HUVEC at lower levels consistent with WT WNV NS1 (Fig. 1E, 1F). We expanded this chimeric NS1 approach to include DENV and ZIKV NS1 and found that while constructs with ZIKV NS1 wing significantly diminished binding to HPMEC, the constructs with DENV NS1 wing did not gain binding to HPMEC comparably to WT DENV NS1 (Fig. 1H, J), possibly due to differential effects of interdomain interactions between flaviviruses. Overall, these results indicate that

the tissue-specific patterns of flavivirus NS1 binding to endothelial cells are driven by the wing domain of NS1.

The wing and β-ladder domains of flavivirus NS1 proteins are necessary for inducing endothelial hyperpermeability

Following binding to endothelial cells, DENV NS1 is taken up by cells via clathrin-mediated endocytosis, trafficks to endosomes, and activates enzymes that degrade the endothelial glycocalyx and disrupt intercellular junctional complexes (7, 10, 31). This results in disruption of endothelial barrier integrity, making endothelial cells hyperpermeable to solutes and liquids. We have previously shown that DENV NS1 can cause endothelial barrier dysfunction by inducing endothelial hyperpermeability independently of the virus (7, 30). Given this finding, we next explored whether the NS1 wing domain that conferred DENV NS1 binding to HPMEC is also responsible for causing HPMEC hyperpermeability. To investigate how different flavivirus NS1 domains influence the capacity of NS1 to trigger endothelial hyperpermeability, we utilized the DENV-WNV NS1 chimeras in a trans-endothelial electrical resistance (TEER) assay. We treated HPMEC seeded in the apical chamber of a trans-well with either WT or chimeric NS1 (2.5 μg/ml) and measured the TEER values between the apical and the basolateral chambers of the transwell (Fig. 3A, B). Consistent with previous observations (33), WT DENV NS1 resulted in significantly greater TEER reduction of HPMEC than WNV NS1, indicating greater endothelial barrier hyperpermeability. Interestingly, the constructs with either the DENV wing or β-ladder domain (i.e. all of the mutant NS1 chimeras) were unable to cause TEER reduction to the same extent as WT DENV NS1, indicating that while the wing domain confers cell binding, both the DENV wing and the DENV β-ladder domains are required for NS1 to trigger endothelial hyperpermeability of HPMEC.

Since we have previously observed that NS1 triggers endothelial hyperpermeability in a dose-dependent manner (7, 8), we tested whether our chimeric NS1 proteins would trigger endothelial hyperpermeability when cells were treated with a higher concentration. We repeated the TEER

experiments using 5 μg/mL of our NS1 proteins (Fig. 3C, D), and observed that the constructs containing the DENV NS1 β-ladder (W-W-**D** and D-W-**D**) caused a decrease in TEER on HPMEC comparably to WT DENV NS1, whereas the constructs containing the WNV β-ladder domain (D-D-**W** and W-D-**W**) did not cause endothelial hyperpermeability, similar to WT WNV NS1. This implicates a role for the DENV β-ladder in inducing endothelial hyperpermeability as measured by TEER, consistent with our previous findings (31, 39).

A 3-amino acid motif in the wing domain of DENV NS1 confers endothelial cell binding specificity between DENV and WNV NS1

While NS1 is highly conserved across the flavivirus genus (40), areas of variability can be found within the wing domain, specifically between amino acid (aa) residues 90 and 120 (Fig. 4A). We have previously identified the same stretch of residues within the NS1 wing domain to be immunodominant, eliciting robust antibody responses in DENV2-infected mice and natural human infections (37). Multiple structural studies have reported a flexible loop structure located near residues 90-120 that is thought to be critical for endothelial cell binding, given its predicted proximity to cell membranes and its exposure on the surface of dimeric NS1 (41–43). This suggests a functional importance that could explain the tissue-specificity of flavivirus NS1. As such, we hypothesized that amino acids within residues 90 to 120 of the wing domain confer tissue-specific endothelial binding.

To test this hypothesis, we aligned the DENV and WNV NS1 sequences to identify differentially conserved residues that were predicted to be surface-exposed, reasoning that these divergent residues may dictate tissue specificity of NS1 (42, 43). We identified five sites of 3-4aa between residues 90 and 120 that contained divergent residues across flaviviruses, which were conserved within each flavivirus (Fig. 4A). To test the involvement of these residues in the differential DENV-WNV NS1 cell binding phenotype, we generated 5 pairs of site-specific mutants that exchanged these motifs between DENV and WNV NS1 (Figs. 4 and 5). We then treated HPMEC with either WT NS1 or site-specific NS1 mutants and measured the levels of NS1 binding to HPMEC by IFA (Fig. 4B). Interestingly, we found

that while 4 pairs retained the binding pattern of their parental NS1 protein, one pair exhibited the opposite pattern. WNV NS1 containing DENV residues 91-93 (WNV-GDI) gained the capacity to bind to HPMEC at comparable levels to WT DENV NS1, whereas the DENV NS1 containing residues 91-93 from WNV NS1 (DENV-EKQ) had reduced capacity to bind to HPMEC, exhibiting levels similar to WT WNV NS1 (Fig. 4B, C). These results suggest that residues 91-93 of DENV NS1 form a motif that contributes to the DENV-WNV tissue-specific endothelial cell binding pattern we observe.

To determine if residues 91-93 conferring NS1 cell binding specificity between DENV/WNV also dictate the capacity of DENV/WNV NS1 to trigger endothelial hyperpermeability, we conducted a TEER assay on HPMEC with NS1 mutants swapped at residues 91-93 and 101-103 for comparison (Fig. 4D). Similar to our observations above, at low NS1 levels (2.5 μg/mL), only WT DENV NS1 was able to induce endothelial hyperpermeability, in contrast to WT WNV and mutants from the DENV/WNV 91-93 and 101-103 swaps that did not noticeably alter permeability, suggesting that while the residues in the wing domain are important for inducing endothelial hyperpermeability, they alone are not sufficient.

We next repeated the TEER experiments at 5μg/mL to confirm if the wing deficiency phenotype of DENV NS1 could be overcome by utilization of a higher dose of NS1 (Fig. 4E). WT DENV NS1 and NS1 constructs containing WNV motifs of either residues 91-93 and 101-103 (both containing DENV β-ladder) were able to trigger endothelial hyperpermeability, whereas WT WNV NS1 caused less TEER decrease, and WNV NS1 constructs containing DENV NS1 motifs of both residues 91-93 and 101-103 (both containing WNV β-ladder) remained unable to cause TEER decrease. Together, these results are consistent with the previous TEER data involving NS1 domain chimeras (Fig. 3), where at the higher NS1 concentration of 5 μg/mL, the constructs containing DENV β-ladder triggered endothelial hyperpermeability.

The wing domain of DENV NS1 confers NS1-induced vascular leak *in vivo*

To explore if the tissue-specific NS1-endothelial cell interactions we observed *in vitro* could be recapitulated *in vivo*, we next asked which NS1 domains were required for tissue-specific vascular leak

in vivo. We used a mouse model of localized dermal leak, in which we have previously shown that DENV NS1 causes significantly higher leak than WNV NS1 (30). We shaved the hair from the back (dorsal side) of wild-type C57BL/6 mice and administered injections intradermally (ID): PBS as baseline vehicle control, WT NS1, and DENV-WNV NS1 chimeras. Immediately following ID injections, we retro-orbitally administered dextran conjugated to Alexa-680. Two hours post-NS1 treatment, we excised the dorsal dermis and used a fluorescent scanner to measure the extent of vascular leak as indicated by dextran-associated fluorescence, since dextran is a small molecule that can extravasate into tissues (Fig. 6A, B).

Using this model, we found that the NS1 chimeras containing DENV wing domain (D-**D**-W and W-**D**-W) caused comparable levels of leak as WT DENV NS1, which is significantly higher leak than the leak caused by WT WNV NS1 (Fig. 6C). Conversely, the NS1 chimeras containing WNV wing domain – and DENV β-ladder (W-**W**-D and D-**W**-D) – caused leak comparable to WT WNV NS1, and significantly less than WT DENV NS1. These data suggest that the DENV NS1 wing is driving NS1-induced vascular leak in the dorsal dermis of mice *in vivo*.

Since we identified residues 91-93 of DENV as a determinant of wing-mediated endothelial hyperpermeability *in vitro*, we asked whether this motif was also a determinant for wing-mediated dermal leak *in vivo*. Using the same dermal leak model as above, we intradermally injected PBS, WT NS1 proteins, and DENV NS1 with WNV NS1 residues 91-93 and *vice versa*, followed by retro-orbital administration of Dextran-A680 (Fig. 6D). We found that WNV NS1 with DENV residues 91-93 gained the ability to trigger vascular leak at comparable levels as WT DENV NS1, while DENV NS1 with WNV residues 91-93 caused significantly less leak, comparable to WT WNV NS1 (Fig. 6E). Taken together, these results suggest that the DENV NS1 wing domain, along with residues 91-93 (GDI), are required to trigger localized vascular leak in this *in vivo* model.

Discussion

In this study, we determined that both the wing and β-ladder domains of flavivirus NS1 proteins drive differential interactions with human endothelial cells, with the wing influencing binding to endothelial cells and the β-ladder involved in inducing endothelial hyperpermeability *in vitro*. We further identified residues 91 to 93 (GDI) within the flexible loop of the DENV NS1 wing domain as a critical molecular determinant for tissue-specific NS1-endothelial cell binding. Finally, we showed that the wing domain, along with the GDI motif, also dictate the capacity of NS1 to trigger vascular leak *in vivo*. Our finding that the NS1 wing domain contributes to endothelial binding and hyperpermeability is consistent with our previous observations (39) and with studies reporting that in DENV NS1-vaccinated mice, anti-wing antibodies were highly protective against lethal DENV infection (37, 44). While in its cell-bound dimeric form, residues within the 90 to 120 region of the wing domain are expected to interact with the plasma membrane (34, 36, 42, 43), which our findings support. In addition, the hydrophobic residues in the DENV NS1 wing domain have also been implicated to be involved in membrane remodeling (45).

It could be expected that flavivirus NS1 contains both conserved core residues mediating interactions with endothelial cells, as well as divergent residues that confer tissue-specificity. In agreement with this hypothesis, previous work from our group uncovered NS1 residues involved in endothelial cell binding that are conserved across the *Flavivirus* genus (W115-W118-G119); these residues are located in the flexible loop within the wing domain (39). In that study, we mutated the W-W-G residues to alanines; the DENV NS1-WWG mutant bound to HPMEC at lower levels than WT DENV NS1 and had reduced capacity to cause endothelial hyperpermeability in HPMEC. This finding suggests that the highly conserved WWG residues may mediate a baseline level of NS1-endothelial cell binding across all flavivirus NS1 proteins, while the tissue-specificity is likely mediated by non-conserved molecular determinants. The conserved WWG residues contrast the DENV-GDI motif we identified in the present study, which is highly variable among flaviviruses.

One interesting observation in our data was how the DENV-WNV chimeras that bound weakly at 2.5µg/mL to HPMEC (W-**W**-D and D-**W**-D, containing WNV wing domain), at much lower levels than

WT DENV NS1, could induce HPMEC hyperpermeability at comparable levels as WT DENV NS1 at the higher NS1 concentration of 5μg/mL (Figure 2). We observed the same trend again when we tested the capacity of the site-directed mutants to cause endothelial hyperpermeability, where at higher concentrations, the DENV-EKQ mutant NS1 bound at a low level to HPMEC while remaining able to cause HPMEC hyperpermeability, whereas WNV-GDI NS1 bound HPMEC but could not cause HPMEC hyperpermeability. This implicates the β-ladder in conferring endothelial cell hyperpermeability, and is consistent with prior studies that identified residues in the β-ladder as important for endothelial hyperpermeability at a step following endothelial cell binding. A glutamine point mutant of the glycosylated residue N207 (31) and targeted mutation at residues T301, A303, E326, E327 (39), which are in the β-ladder domain, were able to bind to HPMEC, but deficient in causing HPMEC hyperpermeability.

It is important to note that while WT WNV NS1 bound to HPMEC less efficiently than DENV NS1, it did bind at detectable levels, although this level of binding was not sufficient to trigger endothelial hyperpermeability (Fig. 3) (14). In the TEER model used to measure endothelial hyperpermeability *in vitro*, cells are treated with NS1 and left undisturbed over time under static conditions, in contrast to DENV infection *in vivo*, where NS1 travels through the bloodstream with constant blood flow. As a result, when the WNV NS1 and DENV-WNV NS1 chimeras (containing WNV wing but DENV β-ladder) that bound poorly to HPMEC were left undisturbed on HPMEC in TEER assays, we hypothesize that their low-level binding was then sufficient to induce hyperpermeability, which was driven by the DENV β-ladder domain. In the *in vivo* environment, we observed that the vascular leak phenotype was conferred by the wing domain, which is consistent with the observation of wing-driven endothelial binding *in vitro*. This suggests that in the fluid condition of the *in vivo* environment, it is critical for NS1 to have strong interactions with host factors on the cell surface such that NS1 binding, which is mediated by the wing domain, can occur despite blood flow.

Further, the complexity of the *in vivo* condition likely accounts for the discrepancy we observe between the *in vitro* endothelial permeability system and the *in vivo* murine dermal leak model, where

293 constructs containing DENV wing and WNV β-ladder could cause vascular leak *in vivo* despite not
294 causing endothelial hyperpermeability *in vitro*. The *in vitro* TEER assay contains only endothelial cells,
295 whereas in the *in vivo* mouse model, other non-endothelial intrinsic factors may be at play, which could
296 be mediated by the wing domain of NS1. In addition, the kinetics differed in our *in vivo* model of
297 localized leak versus *in vitro* TEER assay. Finally, the NS1 proteins might have different effects on the
298 dermal cells in the *in vivo* system as compared to pulmonary cells in the *in vitro* system. Future studies
299 are needed to fully characterize the relative contribution of non-endothelial factors to NS1-mediated
300 vascular leak.

301 A critical question to address next is the mechanism by which the aa 91-93 motif of the wing domain
302 mediates tissue-specific endothelial cell binding. We propose two ways in which residues 91 to 93 may
303 mediate tissue-specific interactions. One possibility is that the motif directly interacts with specific host
304 factors on the surface of endothelial cells such as glycans or proteins. In particular, the carboxylate side
305 chain of D92 points directly towards the cell surface; it may interact with host factors, distinct from the
306 WWG motif, which may facilitate association with the plasma membrane (Fig. 7). A second possibility is
307 that the aa 91-93 motif modulates the flexibility of the flexible loop containing the WWG motif (39),
308 which is ultimately the site predicted to interact with endothelial cells.

309 On the other side of NS1 tissue-specific interactions lies the host endothelial cell. The endothelial
310 cell surface is made up of the endothelial glycocalyx, which is a network of luminal membrane-bound
311 glycoproteins and proteoglycans with both short, branched carbohydrates and long, unbranched
312 glycosaminoglycan side-chains (47, 48). Glycocalyx components include sialic acid, heparan sulfate,
313 chondroitin sulfate, and hyaluronan (47). The composition and ratio of the components that make up
314 the glycocalyx can vary significantly depending on the tissue of origin of endothelial cells, which in turn
315 can result in differential binding of viral proteins to distinct tissues. As such, different residues in both
316 the aa 91-93 motif and the broader wing domain may influence the interactions with specific types of
317 glycans on different endothelial cells.

Our study begins to uncover the molecular determinants for flavivirus NS1 binding and tissue tropism. We establish the flavivirus NS1 wing domain to be important for binding endothelial cells and causing vascular leak, and in the case of DENV NS1, identify residues 91 to 93 within the wing domain as key determinants driving such interactions. This new molecular insight into what determines flavivirus NS1 tissue specificity is crucial for understanding pan-flaviviral pathogenesis and offers new approaches for antiviral therapies.

Acknowledgements

We thank Dr. Janet Smith at the University of Michigan for her helpful discussions about NS1 structure-function relationship. We also thank Evan Juan, Bryan Castillo-Rojas, and Richard Ruan of the Harris laboratory for their technical assistance. Confocal imaging experiments were conducted on a Zeiss LSM 710 microscope at the CRL Molecular Imaging Center at UC Berkeley, which is supported by the Gordon and Betty Moore Foundation. This study was supported by NIH grant R01 AI124493. S.B.B was supported by the Open Philanthropy Life Science Research Foundation postdoctoral award.

N.L., S.B.B, and E.H. conceived the study. N.L., S.R. and N.T. cloned chimeric NS1 constructs. N.L. and S.R. produced and purified the recombinant NS1 proteins. N.L. performed the experiments and data analysis in this study. S.R. assisted on imaging and image analysis. S.B.B. and E.H. provided project guidance. E.H. acquired funding and provided resources. N.L. wrote the initial manuscript draft. N.L., S.B.B, and E.H. reviewed and edited the manuscript and all authors provided editorial comments.

The authors declare no competing interests.

Materials and Methods

Cell lines

FreeStyle 293F suspension cells (Thermo Fisher Scientific) were used for production of recombinant NS1 proteins. 293F cells were cultured in FreeStyle 293 Expression medium (Thermo Fisher Scientific) containing 1% penicillin/streptomycin (P/S) and grown in a CO_2 incubator at 37°C with 8% CO_2 and maintained on a cell shaker at ~130 rpm. HPMEC (HPMEC-ST1.6r) were kindly donated by Dr. J.C. Kirkpatrick at Johannes Gutenberg University, Germany, and were used for NS1 cell binding and TEER assays. HUVEC were kindly gifted from Dr. Melissa Lodoen at the University of California, Irvine. HUVEC are primary endothelial cells obtained from a single female donor (Lonza). Both HPMEC and HUVEC cell lines were propagated (passages 5–10) and maintained in endothelial growth medium 2 (EGM-2) using the EGM-2 bullet kit from Lonza following the manufacturer's specifications and grown in a CO_2 incubator at 37ºC with 5% CO_2.

NS1 mutagenesis and cloning chimeric NS1 proteins

Chimeric NS1 proteins were produced by amplifying fragments of β-roll, wing, and β-ladder domains from the WT DENV2 NS1 (Thailand/16681), WNV NS1 (NY99), or ZIKV NS1 (Uganda MR766), using primers listed in Table 1. The N-terminus of β-roll and C-terminus of β-ladder primer sequences were flanked with nucleotide bases complementary to the protein expression vector plasmid "pMAB". The pMAB vector encodes a N-terminal CD33 signal sequence and C-terminal 6xHis tag, a kind gift from Dr. Michael Diamond, Washington University at St. Louis. The domain fragments and pMAB vector were fused together using overlap extension PCR. Site-directed NS1 mutants were produced using a site-directed mutagenesis kit (QuikChange XL Site-Directed Mutagenesis Kit, Agilent) following the manufacturer's instructions, with primers listed in Table 1. All mutant NS1 constructs were sequence-verified with 5' and 3' primers that recognize the pMAB vector beyond the mutagenesis insertion region.

368 **NS1 protein production and purification**

369 Plasmids containing WT or mutant NS1 sequence were transfected into FreeStyle 293F cells using
370 polyethylenimine (PEI) (40K) (Sigma) according to the manufacturer's instructions. 48 to 72 hours post-
371 transfection, NS1-containing supernatants were collected, filtered through a 0.45 µm cellulose acetate
372 membrane to remove cell debris, and stored at -80º prior to protein purification. The NS1-containing
373 supernatants were thawed, mixed 1:1 with binding buffer (20 mM sodium phosphate, 500 mM sodium
374 chloride, 20 mM imidazole, pH 7.4), and bound to HisPur cobalt resin (Thermo Fisher Scientific) with
375 shaking for 2 hours at room temperature. The NS1-resin mixture then transferred to a column and
376 washed 5 times in wash buffer (20 mM sodium phosphate, 500 mM sodium chloride, 25 mM imidazole,
377 pH 7.4). NS1 was then eluted from the HisPur cobalt resin with elution buffer (20 mM sodium
378 phosphate, 500 mM sodium chloride, 200 mM imidazole, pH 7.4) over 5 fractions. The purified NS1
379 stocks were then subjected to dialysis against 1X PBS for 48 hours at 4ºC and concentrated using
380 Amicon filters with 10,000 molecular weight cut-off (Millipore). The Pierce BCA protein quantitation kit
381 (Thermo Fisher Scientific) was used to quantify the purified recombinant proteins according to
382 manufacturer's instructions. These proteins were used for all experiments within this study.
383
384 **SDS-PAGE and western blot**
385 Recombinant proteins were collected in protein sample buffer (0.1 M Tris pH 6.8, 4% SDS, 4 mM EDTA,
386 286 mM 2-mercaptoethanol, 3.2 M glycerol, 0.05% bromophenol blue) and then resolved by SDS-
387 PAGE. For native gels, the same protocol was followed except that the sample buffer contained no
388 SDS and 2-mercaptoethanol. Proteins were then transferred onto nitrocellulose membranes and
389 probed with primary antibodies diluted in Tris-buffered saline with 0.1% Tween20 (TBST) containing 5%
390 nonfat dry milk. Membranes and antibodies were incubated overnight rocking at 4°C. The next day,
391 membranes were washed three times with TBST before being probed with anti-mouse HRP secondary
392 antibodies diluted in 5% milk in TBST at a dilution of 1:5,000 at room temperature for 1 hour.
393 Afterwards, membranes were washed with TBST three more times before being developed with ECL

reagents and imaged on a ChemiDoc system with Image Lab software (Bio-Rad). The following antibodies were used: mouse anti-His (MA1-21315, Thermo Scientific), goat anti-mouse HRP (405306, Biolegend).

NS1 cell binding assays

To measure binding of WT and mutant NS1 proteins to HPMEC and HUVEC, $1x10^5$ cells were seeded on glass coverslips in 24-well plates. Cells were allowed to form a fully confluent monolayer for 3 days, with medium change every other day. On the day of experiment, 10 µg/mL (3 µg in 300 µL) of NS1 proteins were prepared in 10 µL medium, then added to the cells. Untreated wells were used as negative controls. NS1 and cells were incubated for 1 hour at 37ºC. Mouse anti-6xHis antibody conjugated to Alexa Fluor 647 (Novus Biologicals) was then added at a dilution of 1:200, together with Hoechst 33342 (Immunochemistry) at a 1:2000 dilution for staining of nuclei, for 30 minutes at 37ºC. Cells were then washed twice in 1X PBS followed by fixation in 4% formaldehyde diluted in 1X PBS (Thermo Fisher Scientific). Coverslips were mounted onto microscope slides on a drop of ProLong Gold (Thermo Fisher Scientific) and imaged using a Zeiss LSM 710 inverted confocal microscope (CRL Molecular Imaging Center, UC Berkeley). Images were processed using ImageJ software.

Trans-endothelial electrical resistance (TEER)

The trans-endothelial electrical resistance assay was used to measure the functional effect of NS1 on endothelial barrier function in HPMEC as previously described (33). Briefly, $1x10^5$ cells (HPMEC) were seeded in 300 µL of medium on the polycarbonate membrane insert of a trans-well (Transwell permeable support, 0.4 µm, 6.5 mm insert; Corning Inc.). The trans-well is placed in a well on a 24-well plate, becoming the apical (upper) chamber. 1.5 mL of media is added to the basolateral (lower) chamber. Cells were allowed to form a monolayer for 3 days with media changes in both apical and basolateral chambers every day, until the inter-chamber electrical resistance reaches about 60Ω difference between trans-wells seeded with (~150Ω) and without cells (~90Ω). On the day of

experiment, 2.5 or 5 µg/mL of indicated NS1 proteins (0.75 or 1.5 µg proteins, respectively) were mixed with media up to 10µL, and added to the apical chambers of the trans-wells. Electrical resistance between the apical and basolateral chambers is measured in ohms using an Epithelial Volt Ohm Meter (EVOM) with an electrode pair (World Precision Instruments), at the times indicated in the figures. Trans-wells containing no cells and untreated trans-wells containing only cells were used as negative controls to calculate the baseline electrical resistance at each timepoint. Relative TEER is calculated as a ratio of resistance values $((\Omega_{experimental} - \Omega_{media\ only}) / (\Omega_{untreated\ cells} - \Omega_{media\ only}))$. For area under the curve (AUC) analyses, the net AUC was taken from all curves using baseline of Y=1.

Mouse model of localized vascular leak

Five- to eight-week-old WT C57BL/6 male mice were purchased from the Jackson Laboratory (Bar Harbor, ME) and maintained under specific pathogen-free conditions at the University of California, Berkeley, Animal Facility. Mice were housed in a controlled temperature environment on a 12-hour light/dark cycle, with food and water provided *ad libitum*. All experimental procedures involving animals were pre-approved by the Animal Care and Use Committee (ACUC) of the University of California, Berkeley. Three to four days prior to experiment, the dorsal dermises of 6- to 10-week-old WT C57BL/6 female mice (Jackson Laboratory) were shaved using hair clippers, and residual hair removed using Nair (Church & Dwight). On the day of experiment, 15 µg of WT or mutant NS1 was mixed with PBS in a total volume 50 µL each. NS1 mixtures and PBS were then injected intradermally (ID) into discrete spots in the shaved mouse dermis. Immediately following ID injections, 25 µg of 10-kDa dextran conjugated to Alexa Fluor 680 (1 mg/mL; Sigma) was delivered intravenously (IV) through the retro-orbital route. Two hours post-injection, mice were euthanized, and the dorsal dermis was removed and placed in Petri dishes. The dermis was then placed on a fluorescent scanner (LI-COR Odyssey CLx Imaging System) to visualize the fluorescence signal accumulation at a wavelength of 700 nm. Vascular leak at the ID injection sites was quantified using Image Studio software (LI-COR Biosciences) as described previously (30, 31).

446

447 **Statistics**

448 All quantitative analyses were conducted, and all data were plotted, using GraphPad Prism 9 software.
449 Experiments were repeated at least 3 times, to ensure reproducibility. All experiments were designed
450 and performed with both positive and negative controls (indicated in the figures), which were used for
451 inclusion/exclusion determination. For immunofluorescence microscopy experiments, images of
452 random fields were captured. For all experiments with quantitative analysis, data are displayed as
453 mean ± standard error of the mean (SEM). All cell binding and TEER quantitative data were analyzed
454 using a One-way ANOVA analysis with Tukey's multiple comparisons test. For the localized dermal
455 leak experiments, a non-parametric, unpaired Mann-Whitney U test was used to determine statistical
456 significance between groups. The resulting p-values from the above statistical tests were displayed as
457 n.s., not significant; $p > 0.05$; *$p < 0.05$; **$p < 0.01$; ***$p < 0.001$; ****$p < 0.0001$.

458 **References**

459

460 1. Bhatt S, Gething PW, Brady OJ, Messina JP, Farlow AW, Moyes CL, Drake JM, Brownstein JS,
461 Hoen AG, Sankoh O, Myers MF, George DB, Jaenisch T, William Wint GR, Simmons CP, Scott
462 TW, Farrar JJ, Hay SI. 2013. The global distribution and burden of dengue. Nature 496:504–507.
463 2. Stanaway JD, Shepard DS, Undurraga EA, Halasa YA, Coffeng LE, Brady OJ, Hay SI, Bedi N,
464 Bensenor IM, Castañeda-Orjuela CA, Chuang T-W, Gibney KB, Memish ZA, Rafay A, Ukwaja
465 KN, Yonemoto N, Murray CJL. 2016. The global burden of dengue: an analysis from the Global
466 Burden of Disease Study 2013. Lancet Infect Dis 16:712–723.
467 3. Pierson TC, Diamond MS. 2020. The continued threat of emerging flaviviruses. Nat Microbiol
468 5:796–812.
469 4. Glasner DR, Puerta-Guardo H, Beatty PR, Harris E. 2018. The Good, the Bad, and the Shocking:
470 The Multiple Roles of Dengue Virus Nonstructural Protein 1 in Protection and Pathogenesis.
471 Annu Rev Virol 5:227–253.
472 5. Srikiatkhachorn A, Mathew A, Rothman AL. 2017. Immune-mediated cytokine storm and its role in
473 severe dengue. Semin Immunopathol 39:563–574.
474 6. Malavige GN, Jeewandara C, Ogg GS. 2020. Dysfunctional Innate Immune Responses and Severe
475 Dengue. Front Cell Infect Microbiol 10:1–9.
476 7. Puerta-Guardo H, Glasner DR, Harris E. 2016. Dengue Virus NS1 Disrupts the Endothelial
477 Glycocalyx, Leading to Hyperpermeability. PLoS Pathog 12:1–29.
478 8. Rastogi M, Singh SK. 2020. Zika virus NS1 affects the junctional integrity of human brain
479 microvascular endothelial cells. Biochimie 176:52–61.
480 9. Hui L, Nie Y, Li S, Guo M, Yang W, Huang R, Chen J, Liu Y, Lu X, Chen Z, Yang Q, Wu Y. 2020.
481 Matrix metalloproteinase 9 facilitates Zika virus invasion of the testis by modulating the integrity
482 of the blood-testis barrier. PLoS Pathog 16:1–22.
483 10. Puerta-Guardo H, Tabata T, Petitt M, Dimitrova M, Glasner DR, Pereira L, Harris E. 2020. Zika

Virus Nonstructural Protein 1 Disrupts Glycosaminoglycans and Causes Permeability in Developing Human Placentas. J Infect Dis 221:313–324.

11. Singh S, Anupriya MG, Modak A, Sreekumar E. 2018. Dengue virus or NS1 protein induces trans-endothelial cell permeability associated with VE-Cadherin and RhoA phosphorylation in HMEC-1 cells preventable by Angiopoietin-1. J Gen Virol 1–13.

12. Beatty PR, Puerta-Guardo H, Killingbeck SS, Glasner DR, Hopkins K, Harris E. 2015. Dengue virus NS1 triggers endothelial permeability and vascular leak that is prevented by NS1 vaccination. Sci Transl Med 7:1–11.

13. Modhiran N, Watterson D, Muller DA, Panetta AK, Sester DP, Liu L, Hume DA, Stacey KJ, Young PR. 2015. Dengue virus NS1 protein activates cells via Toll-like receptor 4 and disrupts endothelial cell monolayer integrity. Sci Transl Med 7:1-10.

14. Wessel AW, Dowd KA, Biering SB, Zhang P, Edeling MA, Nelson CA, Funk KE, DeMaso CR, Klein RS, Smith JL, Cao TM, Kuhn RJ, Fremont DH, Harris E, Pierson TC, Diamond MS. 2021. Levels of Circulating NS1 Impact West Nile Virus Spread to the Brain. J Virol 95.

15. Siemann D, Strange D, Maharaj P, Shi PY, Verma S. 2017. Zika Virus Infects Human Sertoli Cells. J Virol 91:1–17.

16. Flamand M, Megret F, Mathieu M, Lepault J, Rey FA, Deubel V. 1999. Dengue Virus Type 1 Nonstructural Glycoprotein NS1 Is Secreted from Mammalian Cells as a Soluble Hexamer in a Glycosylation-Dependent Fashion. J Virol 73:6104–6110.

17. Gutsche I, Coulibaly F, Voss JE, Salmon J, d'Alayer J, Ermonval M, Larquet E, Charneau P, Krey T, Megret F, Guittet E, Rey FA, Flamand M. 2011. Secreted dengue virus nonstructural protein NS1 is an atypical barrel-shaped high-density lipoprotein. Proc Natl Acad Sci 108:8003–8008.

18. Muller DA, Young PR. 2013. The flavivirus NS1 protein: Molecular and structural biology, immunology, role inpathogenesis and application asadiagnostic biomarker. Antiviral Res 98:192–208.

510 19. Edeling MA, Diamond MS, Fremont DH. 2014. Structural basis of Flavivirus NS1 assembly and
511 antibody recognition. Proc Natl Acad Sci 111:4285–4290.
512 20. Young PR, Hilditch PA, Bletchly C, Halloran W. 2000. An Antigen Capture Enzyme-Linked
513 Immunosorbent Assay Reveals High Levels of the Dengue Virus Protein NS1 in the Sera of
514 Infected Patients. J Clin Microbiol 38:1053–1057.
515 21. Libraty DH, Young PR, Pickering D, Endy TP, Kalayanarooj S, Green S, Vaughn DW, Nisalak A,
516 Ennis FA, Rothman AL. 2002. High Circulating Levels of the Dengue Virus Nonstructural Protein
517 NS1 Early in Dengue Illness Correlate with the Development of Dengue Hemorrhagic Fever. J
518 Infect Dis 186:1165–1168.
519 22. Modhiran N, Watterson D, Blumenthal A, Baxter AG, Young PR, Stacey KJ. 2017. Dengue virus
520 NS1 protein activates immune cells via TLR4 but not TLR2 or TLR6. Immunol Cell Biol 95:491–
521 495.
522 23. Avirutnan P, Fuchs A, Hauhart RE, Somnuke P, Youn S, Diamond MS, Atkinson JP. 2010.
523 Antagonism of the complement component C4 by flavivirus nonstructural protein NS1. J Exp
524 Med 207:793–806.
525 24. Avirutnan P, Hauhart RE, Somnuke P, Blom AM, Diamond MS, Atkinson JP. 2011. Binding of
526 Flavivirus Nonstructural Protein NS1 to C4b Binding Protein Modulates Complement Activation. J
527 Immunol 187:424–433.
528 25. Chung KM, Liszewski MK, Nybakken G, Davis AE, Townsend RR, Fremont DH, Atkinson JP,
529 Diamond MS. 2006. West Nile virus nonstructural protein NS1 inhibits complement activation by
530 binding the regulatory protein factor H. Proc Natl Acad Sci 103:19111–19116.
531 26. Malavige GN, Ogg GS. 2017. Pathogenesis of vascular leak in dengue virus infection.
532 Immunology 151:261–269.
533 27. Riswari SF, Tunjungputri RN, Kullaya V, Garishah FM, Utari GSR, Farhanah N, Overheul GJ,
534 Alisjahbana B, Gasem MH, Urbanus RT, de Groot PG, Lefeber DJ, van Rij RP, van der Ven A,
535 de Mast Q. 2019. Desialylation of platelets induced by Von Willebrand Factor is a novel

536 mechanism of platelet clearance in dengue. PLOS Pathog 15:e1007500.
537 28. Chao C-H, Wu W-C, Lai Y-C, Tsai P-J, Perng G-C, Lin Y-S, Yeh T-M. 2019. Dengue virus
538 nonstructural protein 1 activates platelets via Toll-like receptor 4, leading to thrombocytopenia
539 and hemorrhage. PLOS Pathog 15:e1007625.
540 29. Avirutnan P, Zhang L, Punyadee N, Manuyakorn A, Puttikhunt C, Kasinrerk W, Malasit P,
541 Atkinson JP, Diamond MS. 2007. Secreted NS1 of dengue virus attaches to the surface of cells
542 via interactions with heparan sulfate and chondroitin sulfate E. PLoS Pathog 3:1798–1812.
543 30. Glasner DR, Ratnasiri K, Puerta-Guardo H, Espinosa DA, Beatty PR, Harris E. 2017. Dengue
544 virus NS1 cytokine-independent vascular leak is dependent on endothelial glycocalyx
545 components. PLoS Pathog 13:1–22.
546 31. Wang C, Puerta-Guardo H, Biering SB, Glasner DR, Tran EB, Patana M, Gomberg TA, Malvar C,
547 Lo NTN, Espinosa DA, Harris E. 2019. Endocytosis of flavivirus NS1 is required for NS1-
548 mediated endothelial hyperpermeability and is abolished by a single N-glycosylation site
549 mutation. PLOS Pathog 15:e1007938.
550 32. Barbachano-Guerrero A, Endy TP, King CA. 2020. Dengue virus non-structural protein 1
551 activates the p38 MAPK pathway to decrease barrier integrity in primary human endothelial cells.
552 J Gen Virol 101:484–496.
553 33. Puerta-Guardo H, Glasner DR, Espinosa DA, Biering SB, Patana M, Ratnasiri K, Wang C, Beatty
554 PR, Harris E. 2019. Flavivirus NS1 Triggers Tissue-Specific Vascular Endothelial Dysfunction
555 Reflecting Disease Tropism. Cell Rep 26:1598-1613.e8.
556 34. Akey ADL, Brown WC, Dutta S, Konwerski J, Jose J. 2014. Flavivirus NS1 crystal structures
557 reveal a surface for membrane association and regions of interaction with the immune system.
558 Science (80-) 343:1–31.
559 35. Brown WC, Akey DL, Konwerski JR, Tarrasch JT, Skiniotis G, Kuhn RJ, Smith JL. 2016.
560 Extended surface for membrane association in Zika virus NS1 structure. Nat Struct Mol Biol
561 23:865–867.

562 36. Xu X, Song H, Qi J, Liu Y, Wang H, Su C, Shi Y, Gao GF. 2016. Contribution of intertwined loop
563 to membrane association revealed by Zika virus full-length NS 1 structure . EMBO J 35:2170–
564 2178.
565 37. Hertz T, Beatty PR, MacMillen Z, Killingbeck SS, Wang C, Harris E. 2017. Antibody Epitopes
566 Identified in Critical Regions of Dengue Virus Nonstructural 1 Protein in Mouse Vaccination and
567 Natural Human Infections. J Immunol 198:4025–4035.
568 38. Lai YC, Chuang YC, Liu CC, Ho TS, Lin YS, Anderson R, Yeh TM. 2017. Antibodies Against
569 Modified NS1 Wing Domain Peptide Protect Against Dengue Virus Infection. Sci Rep 7:1–15.
570 39. Biering S, Akey DL, Wong MP, Brown WC, Lo NTN, Puerta-guardo H, Tramontini F, Sousa G De,
571 Wang C, Konwerski JR, Espinosa DA, Bockhaus NJ, Glasner DR, Li J, Blanc SF, Juan EY,
572 Elledge SJ, Mina MJ, Beatty PR, Smith JL, Harris E. 2021. Structural basis for antibody inhibition
573 of flavivirus NS1–triggered endothelial dysfunction. Science (80-) 200:194–200.
574 40. Rastogi M, Sharma N, Singh SK. 2016. Flavivirus NS1: A multifaceted enigmatic viral protein.
575 Virol J 13:1–10.
576 41. Akey DL, Brown WC, Dutta S, Konwerski J, Jose J, Jurkiw TJ, DelProposto J, Ogata CM,
577 Skiniotis G, Kuhn RJ, Smith JL. 2014. Flavivirus NS1 structures reveal surfaces for associations
578 with membranes and the immune system. Science (80-) 343:881–885.
579 42. Akey DL, Brown WC, Jose J, Kuhn RJ, Smith JL. 2015. Structure-guided insights on the role of
580 NS1 in flavivirus infection. BioEssays 37:489–494.
581 43. Brown WC, Akey DL, Konwerski JR, Tarrasch JT, Skiniotis G, Kuhn RJ, Smith JL. 2016.
582 Extended surface for membrane association in Zika virus NS1 structure. Nat Struct Mol Biol
583 23:865–867.
584 44. Lai YC, Chuang YC, Liu CC, Ho TS, Lin YS, Anderson R, Yeh TM. 2017. Antibodies Against
585 Modified NS1 Wing Domain Peptide Protect Against Dengue Virus Infection. Sci Rep 7:1–15.
586 45. Ci Y, Liu ZY, Zhang NN, Niu Y, Yang Y, Xu C, Yang W, Qin CF, Shi L. 2020. Zika NS1-induced
587 ER remodeling is essential for viral replication. J Cell Biol 219:1–13.

588 47. Weinbaum S, Tarbell JM, Damiano ER. 2007. The Structure and Function of the Endothelial
589 Glycocalyx Layer. Annu Rev Biomed Eng 9:121–167.
590 48. Srikiatkhachorn A, Kelley JF. 2014. Endothelial cells in dengue hemorrhagic fever. Antiviral Res
591 109:160–170.
592
593

Figure Legends

Figure 1. The wing domain of flavivirus NS1 confers binding to endothelial cells.

(A) Schematic representation of chimeric NS1 proteins that exchange wing or β-ladder domains between DENV and WNV NS1. Red box represents DENV NS1, and blue box represents WNV NS1. The notation (e.g., D-D-W) indicates the unique flavivirus NS1 domain at β-roll, wing, β-ladder domains. **(B)** Recombinant WT or chimeric NS1 (10 μg/mL) was added to HPMEC and incubated at 37ºC for 1h. NS1 binding was assessed by immunofluorescence microscopy, and representative images from three experiments are shown. **(C)** Quantification of (B), normalized to untreated controls. **(D, G)** Schematic representation of chimeric NS1 produced with WNV and ZIKV NS1 (D) or DENV and ZIKV NS1 (G), respectively. Green box represents ZIKV NS1. **(E, H)** NS1 binding to HUVEC or HPMEC, as in B. **(F, J)** Quantification of (E) and (H), respectively. MFI, mean fluorescence intensity. Images represent n=3 biological replicates. Scale bars are 100μm. Data plotted as mean ± SEM. *p<0.05, **p<0.01, ***p<0.005, ****p<0.001 by one-way ANOVA with multiple comparisons. Star colors indicate the respective control each construct was compared to.

Figure 2. Production and quality control of flavivirus NS1 chimeric proteins.

Proteins were evaluated by silver stain following SDS-PAGE (A, C, E) and native PAGE (B, D, F). 2μg of each NS1 construct was used. For native gels, proteins were detected using anti-His mAb. **(A)** Silver stain of DENV-WNV NS1 chimeras. **(B)** Native PAGE of DENV-WNV NS1 chimeras. **(C)** Silver stain of WNV-ZIKV NS1 chimeras. **(D)** Native PAGE of WNV-ZIKV NS1 chimeras. **(E)** Silver stain of DENV-ZIKV NS1 chimeras. **(F)** Native PAGE of DENV-ZIKV NS1 chimeras.

Figure 3. The wing and β-ladder domains of flavivirus NS1 are necessary for inducing endothelial cell hyperpermeability.

(A) HPMEC monolayer was seeded in the apical chambers of 24-well trans-well inserts and treated with either WT or chimeric NS1 proteins at 2.5μg/mL. The trans-endothelial electrical resistance (TEER) between the apical and basolateral chamber were measured over time and normalized to the untreated controls at each respective timepoint. **(B)** Quantification of the area between the curve and Y=1.0 in (A) (“area under the curve”), correlating to a decrease in electrical resistance. **(C)** Endothelial permeability assay as in (A), but with the indicated NS1

622 protein at 5μg/mL. **(D)** Area under the curve of (C). A.u., arbitrary units. Data represent at least n=3 biological
623 replicates, plotted as mean ± SEM. *p<0.05, **p<0.01, ***p<0.005, ****p<0.001 by one-way ANOVA with multiple
624 comparisons. Star colors indicate the respective control each construct was compared to.
625
626 **Figure 4. Residues 91-93 of DENV NS1 drive DENV NS1-endothelial cell interactions.**
627 **(A)** Sequence alignment of DENV and WNV NS1 from residue 91 to 120, with black bars indicating the 3-4
628 residue motifs swapped in the site-directed mutants between DENV and WNV NS1. Colors of the residues
629 indicate their similarities based on biochemical properties. **(B)** NS1 binding assay where 10μg/mL of WT or
630 mutant NS1 as indicated were added to HPMEC and imaged using immunofluorescence microscopy. **(C)**
631 Quantification of (B). **(D)** HPMEC monolayer was seeded in the apical chamber of a trans-well and treated with
632 either WT or site-directed mutant NS1 proteins at 2.5μg/mL. Trans-endothelial electrical resistance (TEER) was
633 measured over time, normalized to the untreated controls of respective timepoints. Area-under-curve
634 quantification TEER curves is shown. **(E)** Same as (D) but treating with NS1 proteins at 5.0 μg/mL. Area-under-
635 curve quantification of TEER curves is shown. All data in this figure are from at least 3 biological replicates,
636 plotted as mean ± SEM. *p<0.05, **p<0.01, ***p<0.005, ****p<0.001 by one-way ANOVA with multiple
637 comparisons. a.u., arbitrary units. Star colors indicate the respective control each construct has been compared to.
638
639 **Figure 5. Production and quality control of flavivirus NS1 site-directed mutants.**
640 Proteins were evaluated by silver stain following SDS-PAGE gel (A) and native PAGE (B, C). 2μg of each NS1
641 construct was used. For native gels, proteins were detected using anti-His mAb. Top row labels indicate the
642 flavivirus NS1 backbone. Numbering under bands refer to the residues that were swapped between DENV and
643 WNV NS1. **(A)** Silver stain of site-directed NS1 mutants between DENV and WNV NS1. **(B, C)** Native PAGE of
644 site-directed NS1 mutants between DENV and WNV NS1, split into two gels each with respective WT DENV and
645 WNV NS1 controls. WT, wild-type.
646
647 **Figure 6. The wing domain of DENV NS1 and residues 91 to 93 within the wing domain confer NS1-**
648 **induced vascular leak *in vivo*.**

649 **(A, B)** Wild-type C57BL/6J mice were shaved by removing hair from their backs 3 days before experiment. On the
650 day of experiment, PBS, WT and chimeric NS1 proteins (15 μg) were administered intradermally into discrete
651 spots on the shaved dorsal dermis. Immediately following NS1 injections, 25 μg of Dextran conjugated to Alexa
652 Fluor 680 was administered retro-orbitally. Two hours post-injection, the dermis of each mouse was collected and
653 visualized using a fluorescent scanner. Representative images of 4 to 6 mice backs are shown. Chimeric proteins
654 were analyzed in different mice with each mouse containing both positive and negative controls (WT DENV and
655 WNV NS1, respectively). **(C)** Mean fluorescent intensity (MFI) quantification of (A) and (B), normalized to PBS
656 injection. **(D)** Same as (A) and (B), but using site-directed NS1 mutants that exchanged residues 91 to 93
657 between DENV and WNV NS1. Representative image of 4 mice backs are shown. **(E)** MFI quantification of (D),
658 normalized to PBS injection. Data plotted as mean ± SEM. *p<0.05, **p<0.01, ***p<0.005, ****p<0.001 by
659 unpaired Mann-Whitney U test. Star colours indicate the respective control each construct was compared to.
660
661 **Figure 7. DENV NS1 structure depicting location of aa 91-93 GDI motif.**
662 Dimeric DENV2 NS1 structure at 2.89Å (PDB 7K93; Biering*, Akey* *et al*, 2021 [39]) was annotated to show the
663 location of the aa 91-93 GDI motif within the wing domain in spatial and structural reference to the rest of NS1.
664 One monomer is coloured grey while the other monomer is coloured as follows: blue for β-roll, yellow for wing, red
665 for β-ladder, and orange for inter-domain connecting regions. Arrows point towards GDI motif on both monomers,
666 coloured in cyan. Plasma membrane is shown to indicate the position in which NS1 is proposed to interact with.
667 **(A)** and **(B)** are rotated 90º along the Y-axis from each other.

Figure 1

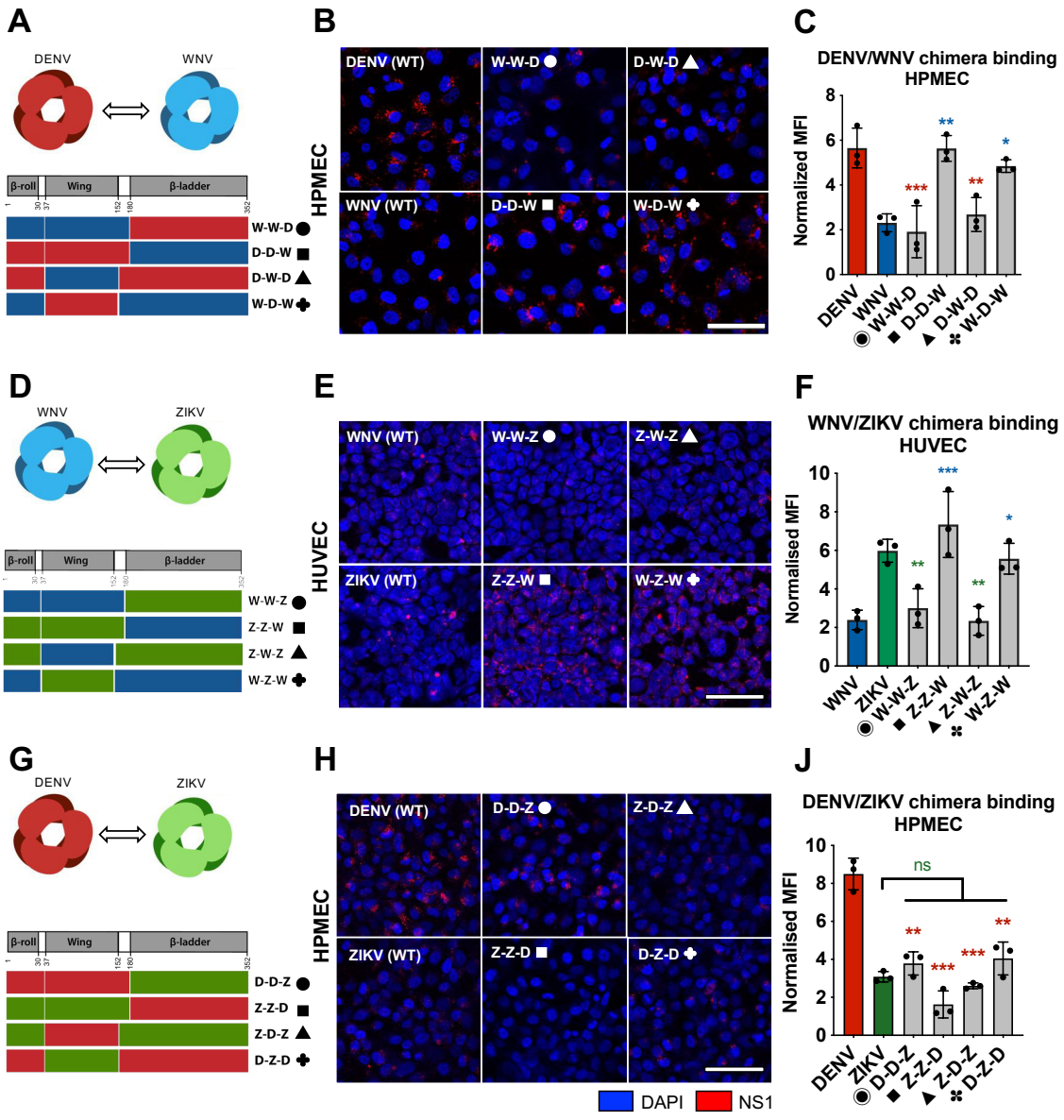

Figure 1. The wing domain of flavivirus NS1 confers binding to endothelial cells.

(A) Schematic representation of chimeric NS1 proteins that exchange wing or β-ladder domains between DENV and WNV NS1. Red box represents DENV NS1, and blue box represents WNV NS1. The notation (e.g., D-D-W) indicates the unique flavivirus NS1 domain at β-roll, wing, β-ladder domains. **(B)** Recombinant WT or chimeric NS1 (10 μg/mL) was added to HPMEC and incubated at 37ºC for 1h. NS1 binding was assessed by immunofluorescence microscopy, and representative images from three experiments are shown. **(C)** Quantification of (B), normalized to

untreated controls. **(D, G)** Schematic representation of chimeric NS1 produced with WNV and ZIKV NS1 (D) or DENV and ZIKV NS1 (G), respectively. Green box represents ZIKV NS1. **(E, H)** NS1 binding to HUVEC or HPMEC, as in B. **(F, J)** Quantification of (E) and (H), respectively. MFI, mean fluorescence intensity. Images represent n=3 biological replicates. Scale bars are 100μm. Data plotted as mean ± SEM. *p<0.05, **p<0.01, ***p<0.005, ****p<0.001 by one-way ANOVA with multiple comparisons. Star colors indicate the respective control each construct was compared to.

Figure 2

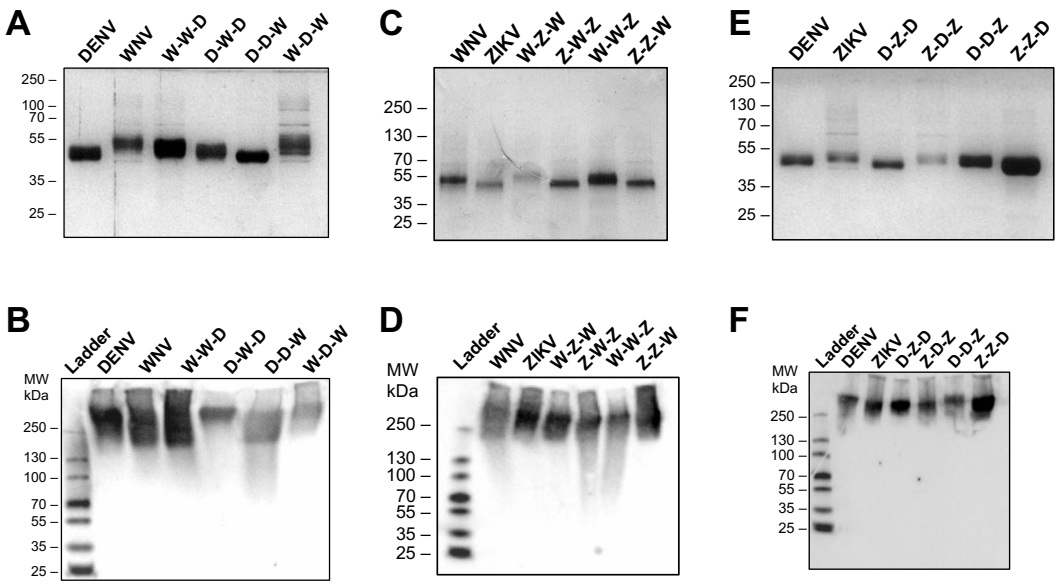

Figure 2. Production and quality control of flavivirus NS1 chimeric proteins.

Proteins were evaluated by silver stain following SDS-PAGE (A, C, E) and native PAGE (B, D, F). 2µg of each NS1 construct was used. For native gels, proteins were detected using anti-His mAb. **(A)** Silver stain of DENV-WNV NS1 chimeras. **(B)** Native PAGE of DENV-WNV NS1 chimeras. **(C)** Silver stain of WNV-ZIKV NS1 chimeras. **(D)** Native PAGE of WNV-ZIKV NS1 chimeras. **(E)** Silver stain of DENV-ZIKV NS1 chimeras. **(F)** Native PAGE of DENV-ZIKV NS1 chimeras.

Figure 3

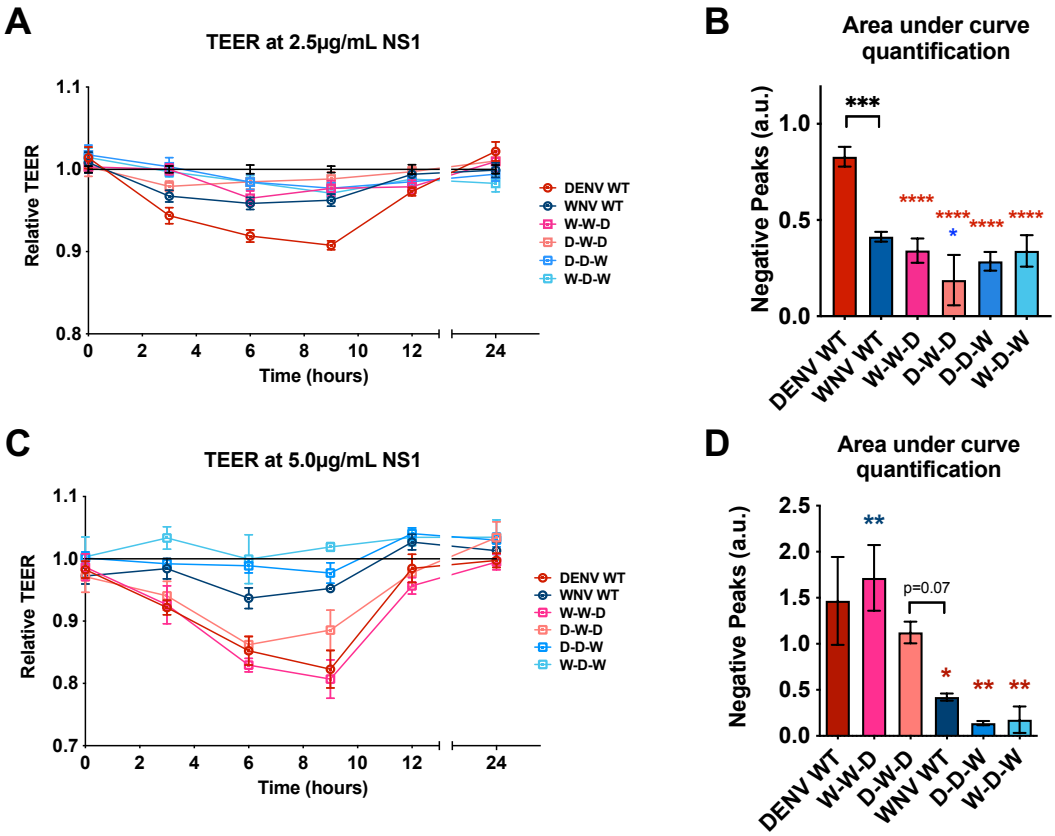

Figure 3. The wing and β-ladder domains of flavivirus NS1 are necessary for inducing endothelial cell hyperpermeability.

(A) HPMEC monolayer was seeded in the apical chambers of 24-well trans-well inserts and treated with either WT or chimeric NS1 proteins at 2.5µg/mL. The trans-endothelial electrical resistance (TEER) between the apical and basolateral chamber were measured over time and normalized to the untreated controls at each respective timepoint. **(B)** Quantification of the area between the curve and Y=1.0 in (A) ("area under the curve"), correlating to a decrease in electrical resistance. **(C)** Endothelial permeability assay as in (A), but with the indicated NS1 protein at 5µg/mL. **(D)** Area under the curve of (C). A.u., arbitrary units. Data represent at least n=3 biological replicates, plotted as mean ± SEM. *p<0.05, **p<0.01, ***p<0.005, ****p<0.001 by one-way ANOVA with multiple comparisons. Star colors indicate the respective control each construct was compared to.

Figure 4

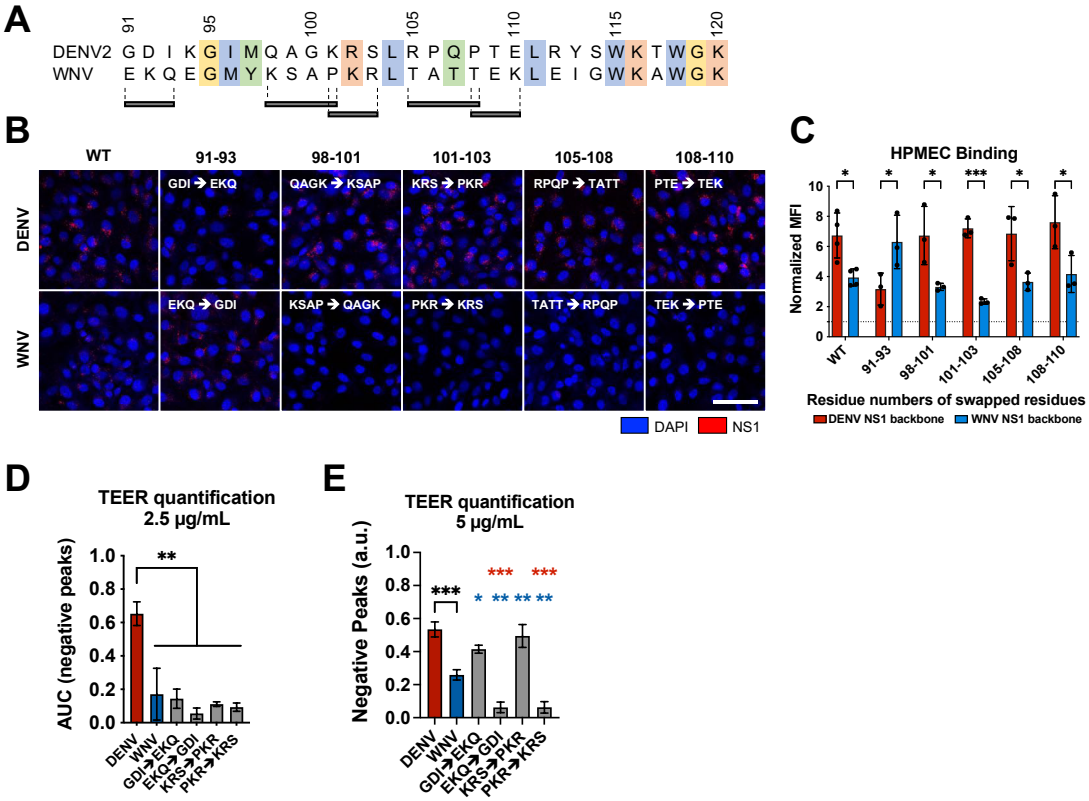

Figure 4. Residues 91-93 of DENV NS1 drive DENV NS1-endothelial cell interactions.

(A) Sequence alignment of DENV and WNV NS1 from residue 91 to 120, with black bars indicating the 3-4 residue motifs swapped in the site-directed mutants between DENV and WNV NS1. Colors of the residues indicate their similarities based on biochemical properties. **(B)** NS1 binding assay where 10µg/mL of WT or mutant NS1 as indicated were added to HPMEC and imaged using immunofluorescence microscopy. **(C)** Quantification of (B). **(D)** HPMEC monolayer was seeded in the apical chamber of a trans-well and treated with either WT or site-directed mutant NS1 proteins at 2.5µg/mL. Trans-endothelial electrical resistance (TEER) was measured over time, normalized to the untreated controls of respective timepoints. Area-under-curve quantification TEER curves is shown. **(E)** Same as (D) but treating with NS1 proteins at 5.0 µg/mL. Area-under-curve quantification of TEER curves is shown. All data in this figure are from at least 3 biological replicates, plotted as mean ± SEM. *p<0.05, **p<0.01, ***p<0.005, ****p<0.001 by one-way ANOVA with multiple comparisons. a.u., arbitrary units. Star colors indicate the respective control each construct has been compared to.

Figure 5

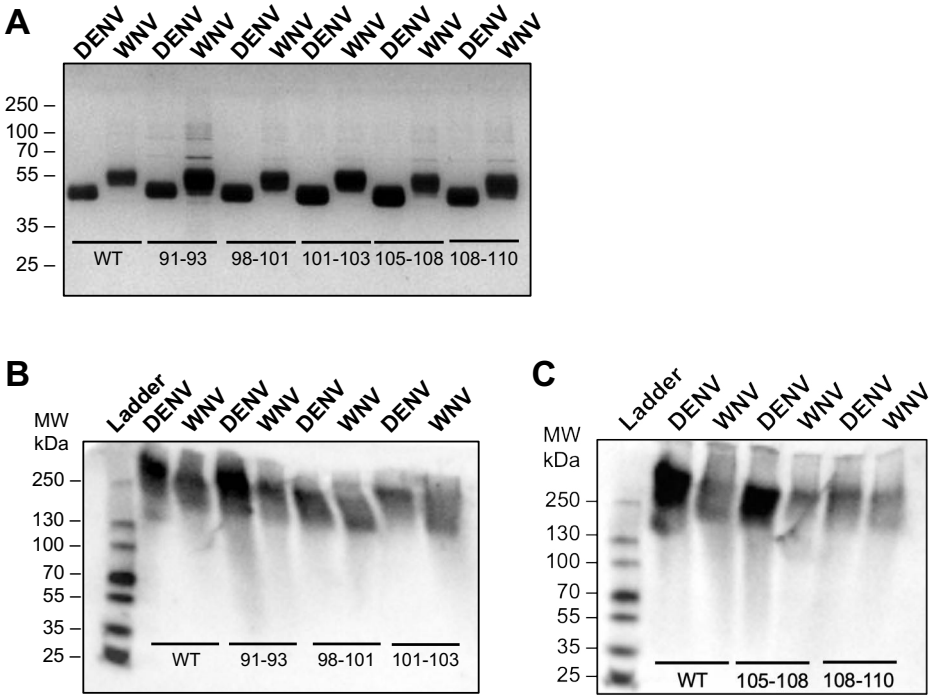

Figure 5. Production and quality control of flavivirus NS1 site-directed mutants.

Proteins were evaluated by silver stain following SDS-PAGE gel (A) and native PAGE (B, C). 2µg of each NS1 construct was used. For native gels, proteins were detected using anti-His mAb. Top row labels indicate the flavivirus NS1 backbone. Numbering under bands refer to the residues that were swapped between DENV and WNV NS1. **(A)** Silver stain of site-directed NS1 mutants between DENV and WNV NS1. **(B, C)** Native PAGE of site-directed NS1 mutants between DENV and WNV NS1, split into two gels each with respective WT DENV and WNV NS1 controls. WT, wild-type.

63 **Figure 6**

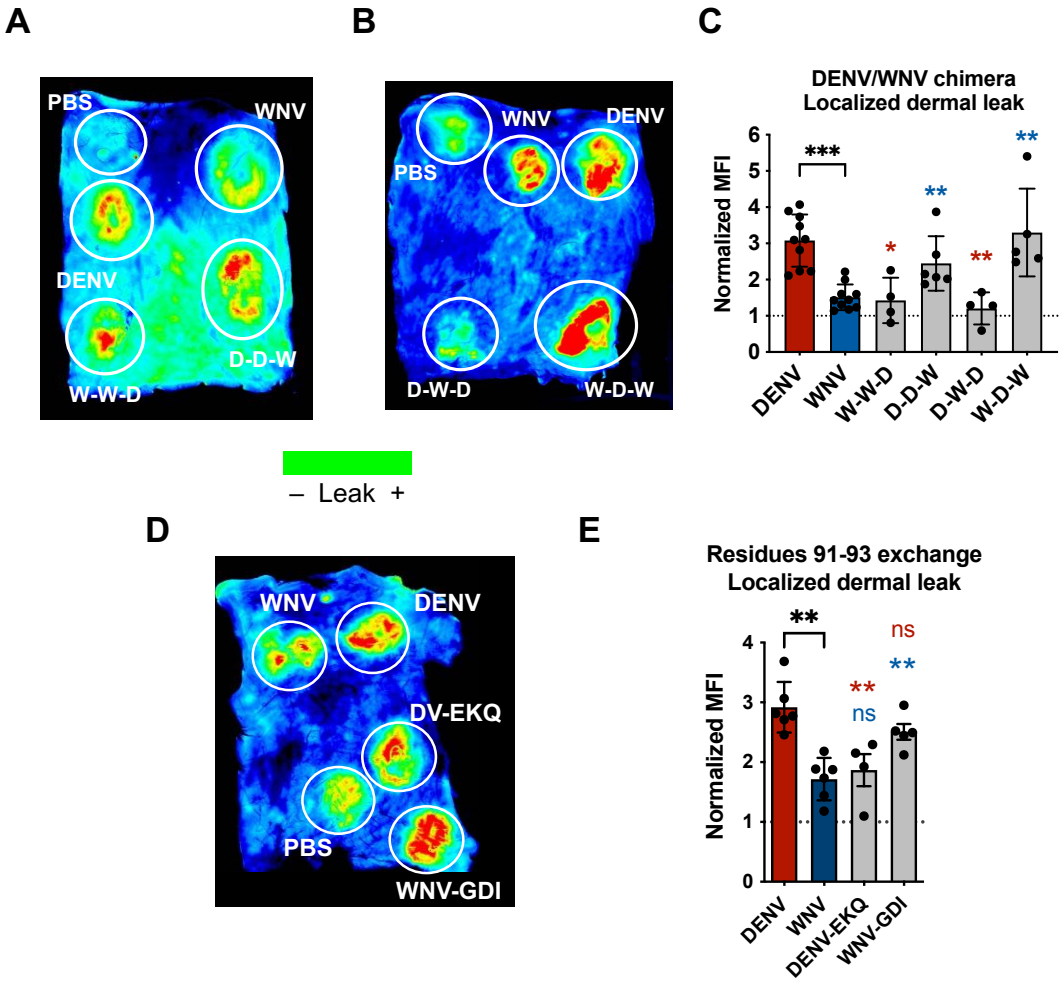

64

65 **Figure 6. The wing domain of DENV NS1 and residues 91 to 93 within the wing domain confer NS1-induced**
66 **vascular leak *in vivo*.**

67 **(A, B)** Wild-type C57BL/6J mice were shaved by removing hair from their backs 3 days before experiment. On the
68 day of experiment, PBS, WT and chimeric NS1 proteins (15 μg) were administered intradermally into discrete spots
69 on the shaved dorsal dermis. Immediately following NS1 injections, 25 μg of Dextran conjugated to Alexa Fluor 680
70 was administered retro-orbitally. Two hours post-injection, the dermis of each mouse was collected and visualized
71 using a fluorescent scanner. Representative images of 4 to 6 mice backs are shown. Chimeric proteins were
72 analyzed in different mice with each mouse containing both positive and negative controls (WT DENV and WNV
73 NS1, respectively). **(C)** Mean fluorescent intensity (MFI) quantification of (A) and (B), normalized to PBS injection.
74 **(D)** Same as (A) and (B), but using site-directed NS1 mutants that exchanged residues 91 to 93 between DENV

and WNV NS1. Representative image of 4 mice backs are shown. **(E)** MFI quantification of (D), normalized to PBS injection. Data plotted as mean ± SEM. *p<0.05, **p<0.01, ***p<0.005, ****p<0.001 by unpaired Mann-Whitney U test. Star colours indicate the respective control each construct was compared to.

78 **Figure 7**

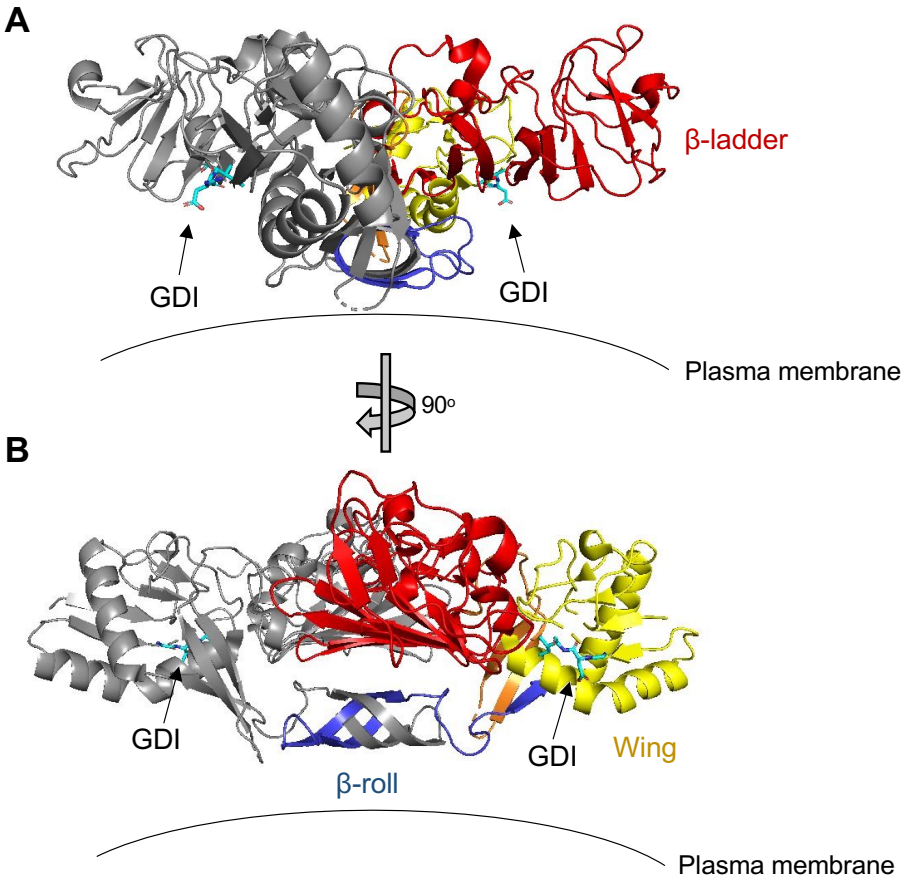

79

80 **Figure 7. DENV NS1 structure depicting location of aa 91-93 GDI motif.**

81 Dimeric DENV2 NS1 structure at 2.89Å (PDB 7K93; Biering*, Akey* *et al*, 2021 [39]) was annotated to show the
82 location of the aa 91-93 GDI motif within the wing domain in spatial and structural reference to the rest of NS1. One
83 monomer is coloured grey while the other monomer is coloured as follows: blue for β-roll, yellow for wing, red for β-
84 ladder, and orange for inter-domain connecting regions. Arrows point towards GDI motif on both monomers,
85 coloured in cyan. Plasma membrane is shown to indicate the position in which NS1 is proposed to interact with. **(A)**
86 and **(B)** are rotated 90º along the Y-axis from each other.

TABLE 1 Primers used for mutagenesis in this study.

Construct	NS1 Backbone	Mutation / Insertion	Primer Direction	Sequence
-	Plasmid pMAB	-	Forward	CTCTAGACCGGTACGCGTGCCGCCACC
-	Plasmid pMAB	-	Reverse	GGATCCCTGCAGCTCGAGTCAGTGATGGTGATGGTGATG
W-W-D	WNV	DENV β-ladder	Forward	AACACAACTGAATGCGACTCAAAACTCATGTCAGCG
	WNV	DENV β-ladder	Reverse	TGACATGAGTTTTGAGTCGCATTCAGTTGTGTTGC
D-D-W	DENV	WNV β-ladder	Forward	AGGATGTATTCTGCGACTCGAAGATCATTGG
	DENV	WNV β-ladder	Reverse	AATGATCTTCGAGTCGCAGAATACATCCTG
D-W-D	DENV	DENV β-roll + WNV wing	Reverse	TAGGCCTTGTGGCGTTTCTGGTTGGAAC
	DENV	DENV β-roll + WNV wing	Forward	AAGTTCCAACCAGAAACGCCACAAGG
	DENV	WNV wing + DENV β-ladder	Reverse	AACTTCCAACGAATTCCAAGCGCG
	DENV	WNV wing + DENV β-ladder	Forward	ATCGCGCTTGGAATTCGTTGGAAGTTG
W-D-W	WNV	WNV β-roll + DENV wing	Reverse	GTTTTGAAGGGGATTCAGGGTAATACTTGTAC
	WNV	WNV β-roll + DENV wing	Forward	GTACAAGTATTACCCTGAATCCCCTTCAAAAC
	WNV	DENV wing + WNV β-ladder	Reverse	TCCACTTCTAAGCTATTCCAAGCTC
	WNV	DENV wing + WNV β-ladder	Forward	TAGAGCTTGGAATAGCTTAGAAGTGG
W-Z-W	WNV	WNV β-roll + ZIKV wing	Reverse	TCTACGGGGGGATTCAGGGTAATAC
	WNV	WNV β-roll + ZIKV wing	Forward	TATTACCCTGAATCCCCCCGTAGATTGG
	WNV	ZIKV wing + WNV β-ladder	Reverse	TCCACTTCTAAGCTGTTCCATGCTCTATG
	WNV	ZIKV wing + WNV β-ladder	Forward	ATAGAGCATGGAACAGCTTAGAAGTGGAGG
Z-W-Z	ZIKV	ZIKV β-roll + WNV wing	Reverse	TAGGCCTTGTGGCGTGTCAGGATGGTAC
	ZIKV	ZIKV β-roll + WNV wing	Forward	TACCATCCTGACACGCCACAAGG
	ZIKV	WNV wing + ZIKV β-ladder	Reverse	ACAAGAAAGCTATTCCAAGC
	ZIKV	WNV wing + ZIKV β-ladder	Forward	TTGGAATAGCTTTCTTGTGG
W-W-Z	WNV	ZIKV β-ladder	Reverse	AATAACGGCTGGGTCGCATTCAGTTG
	WNV	ZIKV β-ladder	Forward	AACTGAATGCGACCCAGCCGTTATTGG

Z-Z-W	ZIKV	WNV β-ladder	Reverse	TGATCTTCGAATCACACTC
	ZIKV	WNV β-ladder	Forward	AGAGTGTGATTCGAAGATCATTGG
D-Z-D	DENV	DENV β-roll + ZIKV wing	Reverse	ATCTACGGGGGGATTCTGGTTGGAAC
	DENV	DENV β-roll + ZIKV wing	Forward	AGTTCCAACCAGAATCCCCCCGTAGATTGG
	DENV	ZIKV wing + DENV β-ladder	Reverse	TCAACTTCCAACGAGTTCCATGCTCTATG
	DENV	ZIKV wing + DENV β-ladder	Forward	TAGAGCATGGAACTCGTTGGAAGTTG
Z-D-Z	ZIKV	ZIKV β-roll + DENV wing	Reverse	AGTTTTGAAGGGGAGTCAGGATGGTAC
	ZIKV	ZIKV β-roll + DENV wing	Forward	TACCATCCTGACTCCCCTTCAAAAC
	ZIKV	DENV wing + ZIKV β-ladder	Reverse	ACAAGAAAGCTATTCCAAGCTCT
	ZIKV	DENV wing + ZIKV β-ladder	Forward	TAGAGCTTGGAATAGCTTTCTTGTGG
D-D-Z	DENV	ZIKV β-ladder	Reverse	ATAACGGCTGGGTCGCAGAATAC
	DENV	ZIKV β-ladder	Forward	TATTCTGCGACCCAGCCGTTATTG
Z-Z-D	ZIKV	DENV β-ladder	Reverse	ACATGAGTTTTGAATCACACTCTAATGA
	ZIKV	DENV β-ladder	Forward	AGAGTGTGATTCAAAACTCATG

Site-directed mutants	DENV	91-93 EKQ (WNV sequence)	Forward	AACTATTATGACAGAGAAACAGAAAGGAATCATGCAGG
	DENV	91-93 EKQ (WNV sequence)	Reverse	TGCATGATTCCTTTCTGTTTCTCTGTCATAATAGTTAAC
	WNV	91-93 GDI (DENV sequence)	Forward	TAGTGTCGTGGTTGGAGACATCGAGGGAATGTACAAG
	WNV	91-93 GDI (DENV sequence)	Reverse	TTGTACATTCCCTCGATGTCTCCAACCACGACACTAAGG
	DENV	98-101 KSAP (WNV sequence)	Forward	ACATCAAAGGAATCATGAAGTCAGCACCTCGATCTCTGCGGCCTCAGC
	DENV	98-101 KSAP (WNV sequence)	Reverse	TGAGGCCGCAGAGATCGAGGTGCTGACTTCATGATTCCTTTGATGTC
	WNV	98-101 QAGK (DENV sequence)	Forward	AACAGGAGGGAATGTACCAGGCAGGAAAAAAACGCCTCACCGCC
	WNV	98-101 QAGK (DENV sequence)	Reverse	TGGCGGTGAGGCGTTTTTTTCCTGCCTGGTACATTCCCTCCTGTTTC
	DENV	101-103 PKR (WNV)	Forward	TGCAGGCAGGACCTAAACGCCTGCGGCCTCAGC
	DENV	101-103 PKR (WNV)	Reverse	TGAGGCCGCAGGCGTTTAGGTCCTGCCTGCATG

	WNV	101-103 KRS (DV)	Forward	TACAAGTCAGCAAAACGATCTCTCACCGCCACC
	WNV	101-103 KRS (DV)	Reverse	TGGCGGTGAGAGATCGTTTTGCTGACTTGTAC
	DENV	105-108 TATT (WNV)	Forward	AAAACGATCTCTGACCGCCACCACGACTGAGCTGAAG
	DENV	105-108 TATT (WNV)	Reverse	TTCAGCTCAGTCGTGGTGGCGGTCAGAGATCGTTTTCC
	WNV	105-108 RPQP (DV)	Forward	ACCTAAACGCCTCCGGCCTCAGCCCGAAAAATTGGAA
	WNV	105-108 RPQP (DV)	Reverse	TTCCAATTTTTCGGGCTGAGGCCGGAGGCGTTTAGGTG
	DENV	108-110 TEK (WNV)	Forward	TCTGCGGCCTCAGACGGAAAAACTGAAGTATTCATG
	DENV	108-110 TEK (WNV)	Reverse	ATGAATACTTCAGTTTTTCCGTCTGAGGCCGCAG
	WNV	108-110 PTE (DV)	Forward	TCACCGCCACCCCCACTGAGTTGGAAATTGGC
	WNV	108-110 PTE (DV)	Reverse	AGCCAATTTCCAACTCAGTGGGGGTGGCGGTGAG

87